

Impact of Calibration and Position Errors on Astrophysical Parameters of the HI 21cm Signal

Anshuman Tripathi,^{a,1} **Abhirup Datta**,^a **Aishwarya Mazumder**,^b
Suman Majumdar,^{a,c}

^aDepartment of Astronomy, Astrophysics and Space Engineering, Indian Institute of Technology Indore, Indore, India – 453552.

^bJodrell Bank Centre for Astrophysics, Department of Physics and Astronomy, The University of Manchester, Manchester M13 9PL, UK

^cDepartment of Physics, Blackett Laboratory, Imperial College, London SW7 2AZ, U. K

E-mail: anshumantripathi85@gmail.com

Abstract. The Epoch of Reionization (EoR) and Cosmic Dawn (CD) are pivotal stages during the first billion years of the universe, exerting a significant influence on the development of cosmic structure. The detection of the redshifted 21-cm signal from these epochs is challenging due to the dominance of significantly stronger astrophysical foregrounds and the presence of systematics. This work used the 21cm E2E pipeline, followed by simulation methodology described [1] to conduct synthetic observations of a simulated sky model that includes both the redshifted 21-cm signal and foregrounds. A framework was constructed using Artificial Neural Networks (ANN) and Bayesian techniques to directly deduce astrophysical parameters from the measured power spectrum. This approach eliminates the need for explicit telescope effects correction in interferometric arrays such as SKA-Low and HERA. The present work investigates the impact of calibration and position errors on retrieving the redshifted 21-cm power spectrum for the above arrays. We assessed the effects of these inaccuracies on the deduced astrophysical parameters and established acceptable tolerance levels. Based on our results, the calibration error tolerance for ideal signal detection is 0.001 %. However, if the position errors exceed 0.048 arcseconds, the remaining foregrounds would obscure the target signal.

¹Corresponding author.

Contents

1	Introduction	1
2	Astrophysical Components in the Simulation	4
2.1	HI 21cm Maps	4
2.2	Foreground Models	5
3	Synthetic Observations	5
3.1	Telescope Model	5
3.1.1	SKA Low	6
3.1.2	HERA	6
4	Power Spectrum	6
4.1	Theoretical Power Spectrum	7
4.2	Observational Power Spectrum	7
5	Emulating HI 21cm Power Spectrum	8
6	Bayesian Inference of EoR Parameters	10
7	Error Covariances of Power Spectrum	11
8	Result	12
8.1	Perfect Observing Condition	12
8.2	Imperfect Observing Conditions	12
8.2.1	Gain Calibration Errors	14
8.2.2	Position Error	14
9	Summary and Discussion	17
A	Robustness Evaluation of the Emulator-based MCMC Pipeline	18

1 Introduction

The redshifted 21cm line is a potential probe of the early Universe [2–4], mainly from the era post recombination until the universe became fully ionized. Based on the theoretical model, in the first billion years of the Universe, Cosmic Dawn (CD) is when the first star or galaxy will be formed ($30 > z > 12$). These stars and galaxies are formed due to gravitational instability, which causes small-scale fluctuation in the matter density. The UV photons produced by these objects ionized the neutral hydrogen (HI) in the intergalactic medium (IGM). This transition period is known as Epoch of Reionization (EoR) [5–9]. Based on various indirect observations such as quasar absorption [10] at high redshifts, Thompson scattering optical depth [11] suggest that the reionization extended the process and lasted at least til the redshift $z \sim 6$.

The observation of HI 21cm power spectrum using large interferometric arrays currently holds the most significant potential to observe the redshifted HI 21cm line [12–15]. The 21cm

signal inherently encodes information about the underlying dark matter distribution and the properties of the ionizing sources. As a result, it has the potential to trace the history of reionization, reflecting the evolution of the average ionization state of the intergalactic medium (IGM) with redshift during the EoR. Detection of the redshifted HI signal is the key science goal of several ongoing and future experiments. Recently, the detection of a global 21cm signal reported by the Experiment to Detect Global Epoch of Reionization Signature (EDGES) team [16]. However, the detection has been challenged by another independent experiment, SARAS [17, 18]. Besides EDGES and SARAS, there are other independent single antenna experiments like BIGHORNS [19], SCI-HI [20], and LEDA [21] are also aiming to detect the global signal but are yet to report any detection. Conversely, interferometers focusing on statistical fluctuations have yielded significant upper limits on the EoR power spectrum (PS) amplitude. The most sensitive operational interferometers, such as the GMRT, MWA, LOFAR, and HERA, have all established upper limits on the power spectrum amplitude of the signal [22–27], but there has been no confirmed detection of the cosmological HI 21cm signal.

However, observing the 21cm signal is highly challenging due to bright astrophysical foregrounds [13, 28–34]. Additionally, other sources of contamination, such as the Earth’s ionosphere and instrument systematics, make detection even more difficult. The observation of the 21cm signal heavily relies on the accuracy of foreground removal and the use of instruments with high sensitivity and controlled systematics. Over the past decade, several novel methods have been proposed to quantify and mitigate each type of contamination for foreground avoidance and removal [35–42], model the systematics of the instruments [43–46], address calibration effects [47–54], and account for the impact of the Earth’s ionosphere [55–57]. These advancements are paving the way for highly sensitive next-generation interferometers, such as the Hydrogen Epoch of Reionization Array (HERA, [58]) and the Square Kilometer Array (SKA-Low, [59]), to detect the 21-cm signal and characterize the multi-redshift power spectrum (PS). This will result in tighter constraints on astrophysical parameters in the early universe. The forthcoming SKA-Low is specifically designed to have the sensitivity needed to detect the PS precisely and is anticipated to generate tomographic images of the HII regions [60].

The EoR signal can be distinguished from foreground contamination because the EoR signal exhibits a spectral structure and is inherently uniform in spatial wavenumber (k) space, whereas foregrounds are spectrally smooth [61–67]. The foregrounds’ smooth spectral nature, along with the inherent chromaticity of the instruments, limit the contamination to the ‘wedge’ in cylindrical Fourier space (i.e., the 2D power spectrum). The area outside this wedge, where the foregrounds are less prominent than the EoR signal, is referred to as the ‘EoR window.’ However, the interaction between astrophysical foregrounds and the instrument results in the leakage of wedge power into the clean modes of the window, a phenomenon known as ‘mode mixing’. This mode mixing impacts the “EoR window,” the region outside the wedge, complicating the detection process [68]. One major recurring challenge in detecting cosmic signals is improper calibration. In radio astronomy sky-based calibration is commonly used, but CD/EoR observations often produce inaccurate models due to low angular resolutions and noise confusion, resulting in residual errors and hindering target cosmological signal detection [35, 48, 50, 69]. The redundant calibration method, investigated by observatories such as HERA, addresses this by repeatedly measuring the redundant baselines of interferometers to correct for the incoming sky signal and instrumental parameters [70, 71].

The signal-to-noise ratio (SNR) is a crucial factor in detecting faint cosmic signals. [1, 69] suggests that even small calibration errors of 0.1 % can significantly reduce the dynamic range and obscure the signal. Further investigation is needed to determine the tolerance of imperfections, which may lead to noise that obscures the detection of weak signals. This study aims to quantify the necessary tolerance for successfully detecting the redshifted 21-cm signal along with astrophysical parameter from cosmic reionization using various sensitive telescopes. To achieve this, we utilize a hybrid machine learning (ML) approach that integrates artificial neural networks (ANN) with Bayesian methods to analyze the effects of imperfections on observational data and their direct impact on the associated astrophysical parameters.

Over the past few years, machine learning (ML) techniques have seen extensive application in various areas of cosmology and astrophysics, particularly in imaging, statistics and inference. Among these ML techniques, artificial neural networks (ANNs) are commonly used in 21cm cosmology for signal modelling, in both kinds, the global signal [72–74] and the power spectrum [75, 76]. ANNs are also employed to infer parameters linked to the signal directly, bypassing traditional Bayesian approaches in both the global 21cm signal [77–80] and power spectrum [81, 82]. Besides ANNs, other ML algorithms are also widely used in various applications of 21cm cosmology. For example, [83] utilized Convolutional Neural Networks (CNNs) to detect reionization sources in 21-cm maps. In [84], deep learning models were employed to replicate the entire time-evolving 21-cm brightness temperature maps from the reionization epoch. The authors validated their predicted 21-cm maps against brightness temperature maps generated by radiative transfer simulations. [85] employed deep learning with CNNs to directly extract astrophysical parameters from 21-cm images. [86] conducted a comparative analysis of machine learning techniques for predicting the 21-cm power spectrum from reionization simulations. [87] proposes a Convolutional Denoising Autoencoder (CDAE) to recover the Epoch of Reionization (EoR) signal by training on SKA images simulated with realistic beam effects.

In this work, we have developed an emulator using an artificial neural network (ANN) framework. This trained ANN emulator was employed as model statistics to constrain EoR astrophysical parameters from the total observed sky power spectrum, which includes the H α signal and systematic effects, via a Bayesian inference process. The motivation for building ANN emulators arises from the computational challenges in EoR 21cm cosmology. Generating numerous observable model signals for multi-dimensional parameter space to perform Bayesian inference using semi-numerical or radiative transfer methods is computationally intensive. Additionally, incorporating telescope effects through simulated observations further increases the computational expense. To address these challenges, we adopted a formalism already utilized by several groups [75, 76], using emulators for EoR signal modeling instead of actual simulations. To construct the training datasets for the emulators, we performed simulated radio interferometric observations using a 21cm E2E pipeline with two different array configurations: SKA Low core and HERA. This allowed us to calculate the total observed sky power spectrum with telescope effect. We also studied the systematic biases introduced in the observed power spectrum by comparing it with the true power spectrum. Furthermore, we examined how these biases influence parameter extraction and quantified the tolerance levels for calibration and position errors necessary for the successful detection of the H α 21cm signal from the EoR using these sensitive telescopes through Bayesian inferences. This is followup work by [1], which quantified the tolerance for calibration and position errors in detecting the H α 21cm signal using various interferometers by analyzing variations in RMS in the im-

age plane and visually examining the 2D and 1D power spectra. Our research investigates the effects of gain calibration and position errors on astrophysical parameters, quantifying the tolerance levels needed to obtain inferred parameters that closely match the true values. Specifically, this work highlights the impact of these errors on the 21cm signal’s astrophysical parameters when no mitigation techniques are applied to the residual foreground contamination caused by them. Furthermore, we are developing a mitigation pipeline, as outlined by *Beohar E. et al., in prep*, to effectively correct these errors, enabling the accurate inference of the true power spectrum and astrophysical parameters.

The structure of this paper is organized as follows: Section 2 outlines the simulation methodology for the HI signal and provides a description of the foreground models used. Section 3 provides the input parameters and telescope array information for performing synthetic observations. Section 4 discusses the Power Spectrum (PS) estimation. Section 5 covers the emulation details of the PS. Section 6 presents the formulation of Bayesian Inference for EoR parameter estimation. Section 7 outlines the method for calculating error covariances of the PS. Finally, Section 8 presents the results.

2 Astrophysical Components in the Simulation

To perform the synthetic observation using the 21cm E2E pipeline, the sky model provided to the pipeline includes the simulated redshifted 21cm signal along with the point source astrophysical foreground model, as detailed below.

2.1 HI 21cm Maps

To generate 21cm maps for our simulated observation, we use a semi-numerical simulation 21cmFAST [88, 89]. 21cmFAST generates HI 21cm maps by first constructing a matter density field and applying the Zeldovich approximation. It employs the guided excursion set formalism to convert the matter density field at a given redshift into an ionization field, which is subsequently used to derive 21-cm brightness temperature fluctuations. In contrast to a detailed radiative transfer approach, this method employs perturbation theory, excursion set formalism, and analytical prescriptions to generate evolved fields for density, ionization, peculiar velocity, and spin temperature. These fields are subsequently integrated to determine the 21-cm brightness temperature. Instead of relying on a halo finder, the code directly processes the evolved density field, enhancing computational efficiency and minimizing memory consumption. This enables the production of numerous realizations of 21-cm maps, power spectra of brightness temperature, matter density, velocity, spin temperature, and ionization fraction at specific redshifts, all at a very low computational cost.

We simulated lightcones in a 500 Mpc^3 comoving box with 232^3 of grid cells for a range for redshift extent of $8.73 \leq z \leq 9.29$. The constructed lightcone volume is saved on a grid of size $232 \times 232 \times 64$ and projected on a World Coordinate System (WCS) to generate an input signal for simulating observations. For this study, we simulate different lightcones to probe different realizations of reionization history using varying EoR parameters. To simulate these lightcones, we use three key EoR parameters (R_{mfp} , T_{vir} , ζ) which can be tweaked to create different reionization histories. We describe these in detail below following [81]:

- R_{mfp} , Mean Free path of ionizing photon: The ionizing photons travel through the ionized IGM strongly depends on the presence of absorption systems and the sizes of ionized regions [90]. Distance travel by a photon from its source of origin to its

sink within ionized regions is called the mean free path of ionizing photon [91]. R_{mfp} determines the size of the ionized regions.

- T_{vir} , Minimum virial temperature of haloes producing ionizing photons: This represents the minimum mass of haloes producing ionizing photons during the EoR. Usually, T_{vir} is chosen to be larger than 10^4 K such that atomic cooling become effective [92, 93].
- ζ , Ionizing efficiency: Ionizing efficiency refers to the ability of sources, such as stars or galaxies, to convert their energy into ionizing photons that can ionize hydrogen in the intergalactic medium. This is a combination of several degenerate astrophysical parameters and is defined as $\zeta = f_{esc} f_{\star} N_{\gamma} / (1 + n_{rec})$ [94, 95]. Here, f_{esc} is the fraction of ionizing photons escaping from galaxies into the IGM, f_{\star} is the fraction of baryons locked into stars and N_{γ} is the number of ionizing photons produced per baryon in stars and n_{rec} is the mean recombination rate per baryon.

2.2 Foreground Models

The foreground component employed in this study specifically includes compact sources. Two distinct catalogues were utilized: the 400 MHz catalogue derived from the uGMRT observations of the ELAIS N1 field [33] and the Tiered Radio Extragalactic Continuum Simulation (T-RECS, [96]). The sources were repositioned around a declination of -30° . Flux values were transformed to 142 MHz using $S_{\nu} \propto \nu^{-\alpha}$, with an α value of -0.8. The 400 MHz catalog ranged from $100 \mu\text{Jy}$ to 0.6 Jy . T-RECS, simulating the continuum radio sky from 150MHz to 20GHz, models Active Galactic Nuclei (AGNs) and Star-Forming Galaxies (SFGs), incorporating real data for realistic cosmological evolution. The chosen catalogue for this study, covering approximately 3 deg^2 , was derived from the 25 deg^2 T-RECS catalogue, maintaining a flux cut-off similar to the EN1 catalogue. Fluxes at 150 MHz were adjusted to 142 MHz using $\alpha \approx -0.8$, resulting in a catalogue comprising 2522 sources within the selected field of view. Notably, the current analysis excludes a diffuse emission model in the foreground, aiming for simplicity, with future studies planning to integrate diffuse emission models to explore their impact.

3 Synthetic Observations

To conduct synthetic observations, we utilized a 21cm end-to-end (E2E) pipeline [1]. This pipeline employs the OSKAR software package [97] for simulating SKA Low configurations, while the Common Astronomy Software Application (CASA) [98] is used for simulating HERA configurations. In this simulated observation, the sky was observed with a phase center at $\alpha = 15^{\text{h}}00^{\text{m}}00^{\text{s}}$ and $\delta = -30^{\circ}$ for a duration of 4 hours (± 2 hours hour angle). The observing bandwidth of the lightcone spans 8 MHz with a channel separation of 125 kHz. For additional details, refer to Table 1.

3.1 Telescope Model

In this work, we are mainly focused on three different types of telescope model details are described below :

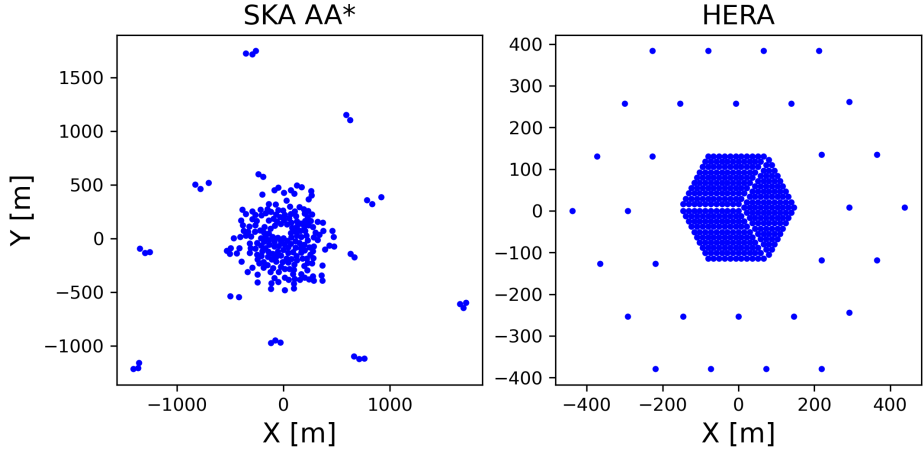


Figure 1. Telescope configurations utilized in the simulation, shown from left to right: SKA Low AA* (with a 2 km central core) and HERA.

3.1.1 SKA Low

The Square Kilometre Array (SKA)¹ is a next-generation, highly sensitive radio telescope designed to detect low-frequency radio signals, such as the 21-cm signal, making it a powerful tool for probing the Epoch of Reionization (EoR) [59]. It is expected to have sufficient sensitivity, with a Signal-to-Noise Ratio (SNR) greater than 1, to create tomographic images of the 21-cm field [60]. The SKA-Low array design includes 512 stations (referred to as AA4), each with a 35-meter diameter, comprising 256 antennas per station. Approximately 50 % of these stations will be concentrated within a 1 km diameter central core, while the remaining stations are distributed along three spiral arms, arranged in clusters of 6 stations with logarithmic spacing. The configuration allows for a maximum baseline of about 73.4 km. In this study, we focus on the AA* SKA-Low layout, which consists of 307 stations with a maximum baseline of 73.4 km. From this layout, we selected all stations located within a 2 km radius (equivalent to a maximum baseline of 2000 meters from the central station), resulting in a subset of 231 stations, array shown in Fig 1.

3.1.2 HERA

The Hydrogen Epoch of Reionization Array (HERA)² is an interferometer designed to detect fluctuations in the 21cm signal from the Cosmic Dawn and Epoch of Reionization [58]. Located in the South African Karoo Radio Astronomy Reserve, HERA will eventually consist of 350 parabolic dishes, each 14 meters in diameter, arranged in a highly redundant configuration—320 in a dense core and 30 as outriggers—as shown in Fig. 1. The instrument operates within the 100–200 MHz frequency range. This study employs the full array of 350 dishes, which provides a maximum baseline of approximately 880 meters.

4 Power Spectrum

A key scientific objective of both ongoing and upcoming radio interferometric arrays is to detect and characterize fluctuations in the brightness temperature of the redshifted 21cm sig-

¹<https://www.skao.int/en/explore/telescopes/ska-low>

²<https://reionization.org/>

Parameters	SKA (AA*)	HERA
Central Frequency	142 MHz (z~9)	142 MHz (z~9)
Bandwidth	8 MHz	8 MHz
Number of frequency channels	64	64
Field of view	4°	4°
Number of array elements (N_a)	231	350
Maximum baseline (m)	~2000	~880
Effective collective area (A_{eff})	~ 962 m^2	~ 154 m^2
Core area of an array (A_{core})	~ 12.57 km^2	~ 0.608 km^2

Table 1. Parameter values used to conduct these synthetic simulations.

nal from the EoR. Various statistical tools are available for these interferometric experiments to calculate these fluctuations in terms of the power spectrum (PS) using both the visibility data [25] and the image plane [26]. In this study, we have calculated the theoretical PS from the image plane and the observed PS from simulated visibility data for different arrays such as SKA Low and HERA, as shown in Fig. 2.

4.1 Theoretical Power Spectrum

The fluctuation of the brightness temperature δT_b for the 21 cm signal can be defined as [99]:

$$\delta T_b(\nu) \sim 27x_{HI}(1 + \delta_m) \left(\frac{H}{\frac{dv_r}{dr} + H} \right) \left(1 - \frac{T_\gamma}{T_S} \right) \times \left(\frac{1+z}{10} \frac{0.15}{\Omega_m h^2} \right)^{1/2} \left(\frac{\Omega_m h^2}{0.023} \right) \left(\frac{\Omega_b h}{0.031} \right) [\text{mK}] \quad (4.1)$$

where, x_{HI} denotes the neutral hydrogen fraction, Ω_m represents the matter overdensity, and H refers to the Hubble parameter. Additionally, dv_r/dr signifies the local gradient of gas velocity along the line of sight, while T_S and T_γ correspond to the spin temperature of the intergalactic medium (IGM) and the temperature of the cosmic microwave background (CMB), respectively.

We can define the dimension 21cm power spectrum as :

$$\Delta^2(k) = \frac{k^3}{2\pi^2} P(\mathbf{k}) \quad (4.2)$$

$P(\mathbf{k})$ can define as

$$\langle \delta T_b(\mathbf{k}) \delta T_b(\mathbf{k}') \rangle = (2\pi)^3 \delta(\mathbf{k} + \mathbf{k}') P(\mathbf{k}) \quad (4.3)$$

where $\delta T_b(k)$ is Fourier conjugate of $\delta T_b(\nu)$.

4.2 Observational Power Spectrum

The interferometric visibility is defined as the correlation between the signals received by a pair of antennas, which is given by [100] :

$$V(\mathbf{U}, \nu) = \iint A(\hat{\mathbf{s}}, \nu) B(\nu) I(\hat{\mathbf{s}}, \nu) e^{-i2\pi\nu \mathbf{U} \cdot \hat{\mathbf{s}}} d\Omega, \quad (4.4)$$

Here, \mathbf{U} represents the baseline vector, while $I(\hat{\mathbf{s}}, \nu)$ and $A(\hat{\mathbf{s}}, \nu)$ correspond to the specific intensity and the antenna beam pattern, respectively, both as functions of frequency (ν). The term $B(\nu)$ denotes the instrumental bandpass response. The unit vector is defined as $\hat{\mathbf{s}} \equiv (l, m, n)$, where l , m , and n are the direction cosines pointing towards the east, north, and zenith, respectively, with $n = \sqrt{1 - l^2 - m^2}$. The solid angle element is given by $d\Omega = \frac{ldm}{\sqrt{1-l^2-m^2}}$. In this study, $A(\hat{\mathbf{s}}, \nu)$ is assumed to be 1, meaning the primary beam effect is not taken into account.

The inverse Fourier transform of $V(\mathbf{U}, \nu)$ along the frequency axis converts the visibility into the delay domain, denoted as τ , resulting in $V(\mathbf{U}, \tau)$. Based on this approach, the cylindrical power spectrum, as described in [61], is expressed as follows:

$$P(\mathbf{k}_\perp, k_\parallel) = \left(\frac{\lambda^2}{2k_B}\right)^2 \left(\frac{X^2 Y}{\Omega B}\right) |V(\mathbf{U}, \tau)|^2, \quad (4.5)$$

where λ represents the wavelength corresponding to the central frequency, k_B is the Boltzmann constant, Ω denotes the primary beam response, and B is the bandwidth. The factors X and Y convert angular and frequency measurements into the transverse co-moving distance $D(z)$ and the co-moving depth along the line of sight, respectively [61]. The term \mathbf{k}_\perp corresponds to the Fourier modes perpendicular to the line of sight, while k_\parallel represents the modes along the line of sight, defined as follows:

$$\mathbf{k}_\perp = \frac{2\pi|\mathbf{U}|}{D(z)} \quad \& \quad k_\parallel = \frac{2\pi\tau\nu_{21}H_0E(z)}{c(1+z)^2}$$

Here, ν_{21} represents the rest-frame frequency of the 21 cm spin-flip transition of HI, while z denotes the redshift corresponding to the observing frequency. The Hubble parameter is given by H_0 , and $E(z) \equiv [\Omega_M(1+z)^3 + \Omega_\Lambda]^{1/2}$. The parameters Ω_M and Ω_Λ correspond to the matter and dark energy densities, respectively.

The 1D power spectrum is derived from the 2D power spectrum by performing a spherical average of $P(\mathbf{k}_\perp, k_\parallel)$ and is given by:

$$\Delta^2(k) = \frac{k^3}{2\pi^2} \langle P(\mathbf{k}) \rangle_k \quad (4.6)$$

where, $k = \sqrt{k_\perp^2 + k_\parallel^2}$.

5 Emulating HI 21cm Power Spectrum

The objective of developing ANN-based emulators for this work is to study the power spectrum, as these emulators can generate efficient and reliable EoR models. These models can then be utilized as substitutes for computationally intensive simulations in Bayesian parameter inference. In addition to this, a non-parametric feature of ANN emulators is the ability to replicate various signal features without relying on their specific parametric characteristics, as they are solely dependent on the training data sets. This capability allows us to utilize the features directly without the need to remove or apply any cleaning algorithms, thereby enabling the inference of associated label parameters. In this study, we are developing emulators by training with different PS observed by different interferometric arrays like SKA Low and HERA. We also train the emulator for the theoretical power spectrum, which one can say is the power spectrum for the perfect array interferometric condition. We use the ANN

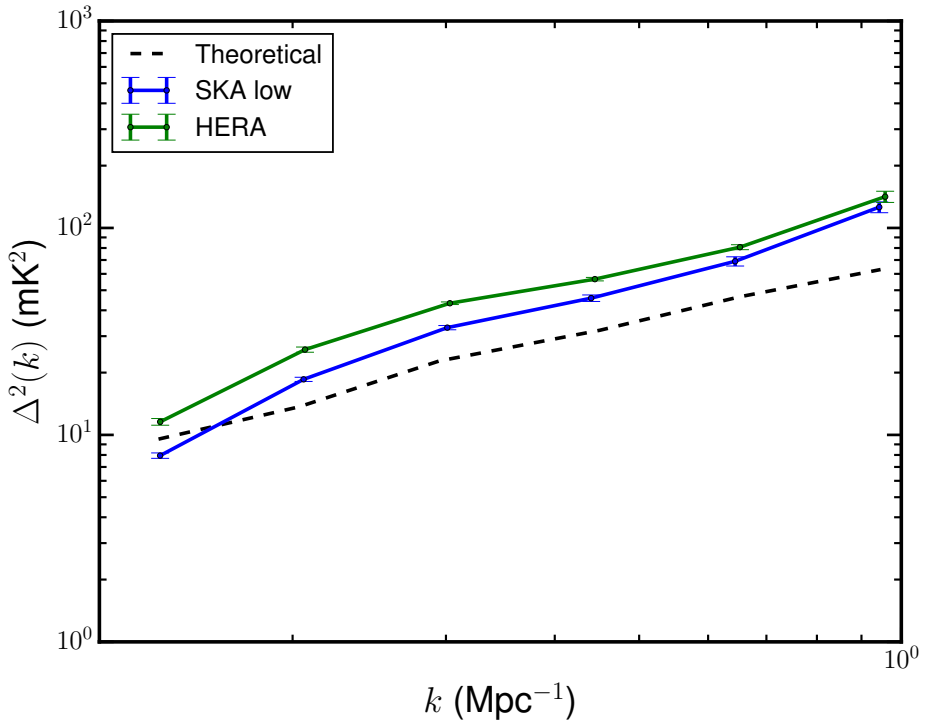


Figure 2. Shows a comparison of the theoretical spherical power spectrum (PS) and the simulated observed PS for the same sky model. The theoretical PS for the signal models is represented by a black dashed line, while the simulated observed PS for different array configurations is plotted with solid lines: blue for SKA-Low and green for HERA, for the same signal mode.

model to build these emulators. To develop ANN architecture, we are using the Python-based deep learning Keras API, and standard sci-kit learn [101]. To achieve significant accurate PS from the emulator for test set of EoR parameter we have to train the emulator with the sufficient number of the training datasets. To construct an optimal training data set, we sample the parameter space with Latin Hypercube Sampling. Latin Hypercube sampling method samples the multi-dimensional parameter space such that no two parameters share the same value in the parameter space, providing an all-unique set of parameters. We sampled the EoR parameters range into 300 grid points using Latin Hypercube sampling to build the training and test datasets. These 300 sample data points given as input to construct the lightcones details are described in section 2.1, which is further used to construct the observed power spectrum using the 21cm E2E pipeline. To develop construct training and test datasets for the theoretical PS, we use 21cmFast. The parameters range we follow to construct the training datasets are $R_{mfp} = (10 \text{ Mpc}, 60 \text{ Mpc})$, $\log(T_{vir}) = (4.5 \text{ K}, 6.0 \text{ K})$, and $\zeta = (10, 60)$. We construct training and test data sets of observed/theoretical power spectrum ($\Delta^2(k)$) by following these sample parameters for 6 different k modes. We use 270 sample data sets to train and validate the ANN model and 30 data sets to test the ANN emulator. We constructed the network architecture by following Python-based Keras' Sequential API. The network consists of an input layer consisting 3 neurons matching with the training 3 EoR key parameter (R_{mfp} , $\log(T_{vir})$, ζ) and two hidden layers with 28 and 14 neurons, respectively, each activated by the 'elu' activation function. The output layer has 6 neurons to predict the observed PS. The input PS data sets are normalized using the 'StandardScaler' function,

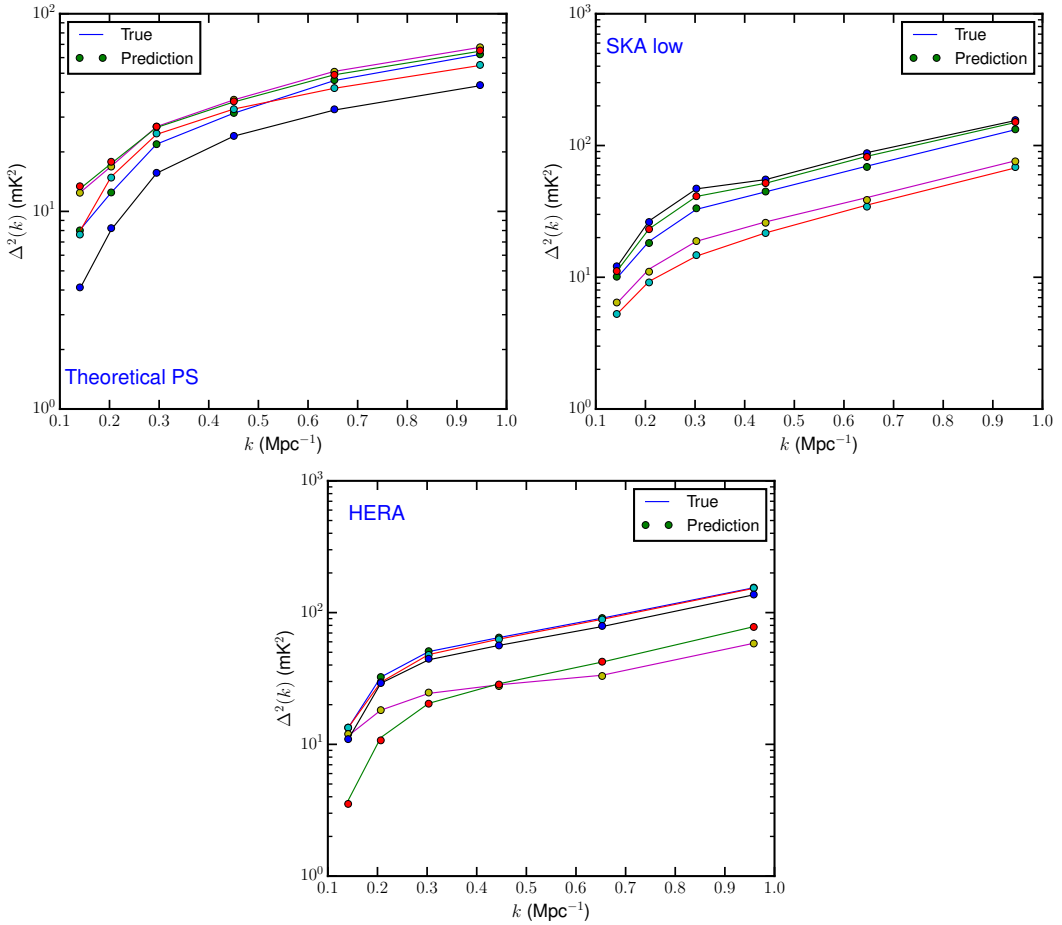


Figure 3. The figure shows a comparison between the simulated true power spectrum (solid lines) and the emulated power spectrum by the ANN (dots). Clockwise from the top left, it presents emulator predictions trained on: theoretical PS, observed PS with SKA-Low and HERA, respectively.

and corresponding EoR parameters are normalized using `MinMaxScaler`, which is available in `sklearn`. We trained this ANN model using different power spectra (PS) observed by various interferometric arrays, such as SKA Low and HERA, to create individual emulators for each array. Fig. 3 presents a comparison between the true test set 21-cm PS, shown as solid lines, and the emulated PS by the ANN, represented by dots. For this comparison, we randomly selected five test sets of power spectra and compared them with the predicted PS from the emulators in each case.

6 Bayesian Inference of EoR Parameters

To constrain the EoR parameters and associated errors in the inferred parameter values, the Bayesian approach is one of the most popular methods. In the Bayesian approach, the posterior distribution of the parameters can be defined using Bayes' theorem :

$$p(\theta|D, M) = \frac{p(D|\theta, M)\Pi(\theta|M)}{p(D|M)} \quad (6.1)$$

where θ represents the parameters, D is data, and M represents a model. The evidence $p(D|M)$ serves as a constant normalization factor for a given model. The posterior distribution is determined solely by the product of the likelihood function $L = p(D|\theta, M)$ and the prior distribution of the parameters θ , denoted as $\Pi(\theta|M)$. For this study, we considered a multivariate Gaussian likelihood which can be expressed as:

$$\ln L = -\frac{1}{2}[\vec{d}_{ref} - \mu]^T[\sigma^2]^{-1}[\vec{d}_{ref} - \mu] - \frac{1}{2}\ln(2\pi \det\{\sigma^2\}) \quad (6.2)$$

where \vec{d}_{ref} represents reference data, μ represents the model observable corresponding to the observable parameters and σ^2 is the error covariance associated with \vec{d}_{ref} .

We design our pipeline to extract the most likely EoR parameter values using MCMC for the given log-likelihood. We used the CosmoHammer [102] Python package, utilizing an affine-invariant [103] Markov Chain Monte Carlo (MCMC) ensemble sampler, to conduct model parameter estimation. To test the performance of the pipeline we input either the binned theoretical 21-cm power spectrum or simulated observed power spectrum.

7 Error Covariances of Power Spectrum

The error estimate in the observables is essential to predict the posterior of the parameters. The EoR 21cm signal has various contamination from the foreground, systematics, noise, calibration errors etc. To estimate the error covariance of the power spectrum (PS), we assume that the foregrounds have been perfectly modeled and entirely removed from the observed signal. The remaining observed signal consists of the EoR 21cm signal and Gaussian thermal noise. Hence, in this analysis, the total covariance (σ_t^2) is defined as the sum of the sample variance (σ_{SV}^2) and the thermal noise variance (σ_N^2).

$$\sigma_t^2(i) = \sigma_{SV}^2(i) + \sigma_N^2(i) \quad (7.1)$$

In this analysis, we assume that the measurements at any two bins are mutually uncorrelated which simplifies the error computation. In this study we use variance instead of covariance to calculate error σ^2 . We estimated the sample variance for the bin average power spectrum $P(k_i)$ by following equation

$$\sigma_{SV}^2(P_i) = [\Delta^2(k_i)]^2/N_{k_i} \quad (7.2)$$

where N_{k_i} denotes the number of measurement at each k-mode. The thermal noise for given radio interferometric array can be estimated using the following equation [104, 105]:

$$\sigma_N^2(P_i) = \frac{k^3}{2\pi^2\sqrt{N_{k_i}}} \left(\frac{2T_{sky}^2 D^2(z) \Delta D \Omega_{FoV}}{B t_{obs} n_p} \left(\frac{A_{eff} A_{core}}{A_{coll}^2} \right) \right) \quad (7.3)$$

where A_{eff} , A_{coll} , and A_{core} denote the effective area, collecting area, and core area, respectively, of the specified radio interferometric array. The symbol t_{obs} signifies the total observation time in hours. Additionally, D and ΔD denote the comoving distance to the redshifts where the center is located and the comoving distance corresponding to a bandwidth B at that comoving distance. T_{sky} denotes the sky temperature calculated using $T_{sky} \sim 180 \left(\frac{\nu}{180\text{MHz}} \right)^{-2.6} \text{K}$ [5], symbol Ω_{FoV} denotes field of view symbol, n_p represents the number of polarization and N_{k_i} denotes the number of measurement at each k-mode.

8 Result

This section describes simulation outcomes and discusses their relevance to actual observations. The results for each considered configuration are detailed in individual sections below.

8.1 Perfect Observing Condition

In this study, we derived astrophysical characteristics from various interferometric arrays' observed power spectra (PS). We assumed that foregrounds were perfectly removed from the observed PS and that there were no calibration or positional errors, as shown in Fig. 2. To achieve this, we simulated observations using the 21cm E2E pipeline with only input HI lightcone maps and calculated the PS from the resulting observed HI visibility. To derive the astrophysical parameters, we employed an emulator-based Markov Chain Monte Carlo (MCMC) pipeline. The advantage of employing this emulator-based MCMC pipeline lies in its ability to reduce computational time significantly. Furthermore, as the emulators are trained on observed power spectra that inherently incorporate telescope effects, they allow for direct parameter inference without the need for separate corrections for these effects. The inferred astrophysical parameters for various interferometric arrays are depicted in Fig.5. For all cases, we found that the two parameters, ζ and T_{vir} , closely matched the actual values. However, the third parameter, R_{mfp} , was not correctly constrained in any of the cases. To investigate this issue, we examined whether the lack of constraint could be due to the effects introduced by the telescope. Additionally, we compared these results with the inferred astrophysical parameters derived from theoretical power spectra. A similar trend was observed in this case as well. Specifically, ζ and T_{vir} closely matched the actual values, as shown in Fig.4. However, R_{mfp} remained unconstrained in all scenarios, which may be attributed to the degeneracy of the R_{mfp} parameter. To further assess the robustness of this pipeline, we inferred parameters for two additional power spectra generated using astrophysical parameters near the boundary values of those used in the training dataset. The inferred parameters for these power spectra are presented in Fig.7, with set 2 on the left and set 3 on the right, as detailed in Appendix A. Similar to the initial case, the astrophysical parameters ζ and T_{vir} were well-constrained and closely aligned with the true values in most instances, as depicted in Fig.7. However, the parameter R_{mfp} remained poorly constrained across both sets.

We also noticed that the power spectrum from set 1, whose astrophysical parameters are around the centre of the boundaries, generated more accurate conclusions across all interferometric measured PS. By contrast, the power spectra generated in close proximity to the boundary values of the astrophysical parameters yielded inferred parameter mean that differed from the actual value. This mismatch could be due to the ANN emulator being trained on restricted datasets. Potential future development of a more precise emulation could involve training it with a more extensive dataset.

8.2 Imperfect Observing Conditions

Sensitive radio observations like the ones targeting the HI signal from CD/EoR is prone to contamination from a large number of sources. Small errors in initial processing steps like calibration can propagate into the final power spectrum estimates, resulting in misinterpretation of the obtained results. In [1], the authors studied the effects of calibration errors and positions errors in the recovery of the 21-cm power spectrum. In this study, we follow up by exploring the effect of such errors on the recovery of astrophysical parameters. The visual

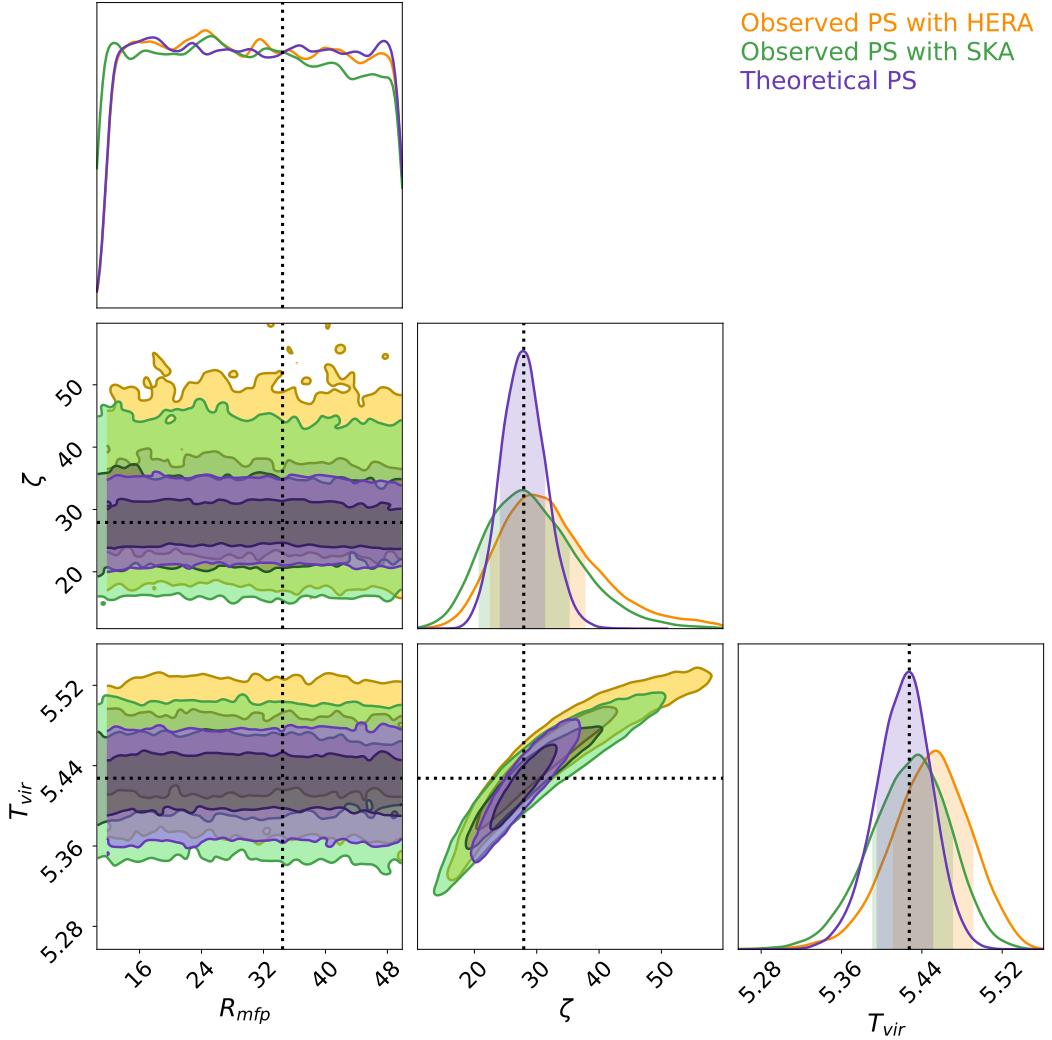


Figure 4. Depicts the posterior distribution of model parameters obtained through power spectrum analysis, comparing the theoretical power spectrum with the observed power spectrum using various interferometric arrays, including SKA Low and HERA. The enclosed areas between the inner and outer contours signify the 1σ and 2σ confidence levels, respectively.

comparison of the PS was previously conducted by [1], where they examined both 2D and 1D residual PS with gain errors and position errors. They also investigated the variation of root mean square (RMS) in the residual image across different percentages of calibration errors and position errors, comparing it with the signal level and thermal noise. In the previous study by [1], it was found that a gain error threshold of 0.01% leads to a high image RMS for both the SKA-Low and HERA interferometric arrays, potentially causing confusion or even obscuring the detection of faint cosmological signals. Similarly, they explored the variation of RMS in the residual image across different position errors, comparing it with the signal level and thermal noise. In their study, [1] found that a position error threshold of $0.48''$ leads to a high image RMS, potentially causing confusion or even obscuring the detection of faint cosmological signals. In our study, we compared the corrupted 1D power spectrum (PS) with the original PS and estimated the astrophysical parameters from the corrupted PS for

both scenarios: when it was corrupted by gain calibration errors and when it was corrupted by position errors.

8.2.1 Gain Calibration Errors

Gain calibration errors were incorporated following equation 1 from [1], applied per antenna rather than per baseline, affecting the entire k range.

SKA Low: To assess the influence of calibration errors on the observed power spectrum (PS) and their subsequent impact on associated astrophysical parameters for SKA-Low, we introduced various gain errors as detailed in [1]. The resulting residual PS was visually compared with the actual PS, depicted in the top left panel of Fig. 5. The parameter obtained from the PS analysis with SKA-Low, incorporating actual signal and PS for gain error residuals, is depicted in the top right panel of Fig. 5. Upon examining the plotted residual PS spectrum, we observed that for gain errors of 0.001 %, the residual PS overlaps with the true PS. For residual PS with gain errors of 0.01%, we observe overlapping at lower k modes, but with minor deviation at higher k modes. However, when deriving astrophysical parameters from the residual power spectrum, we found that for a gain error of 0.001%, the derived parameters match those derived from the true PS. In contrast, for PS with the gain error of 0.01%, the derived parameters exhibit significant differences from the actual values. This indicates that astrophysical parameters are highly sensitive to gain errors, and even minor deviations in the PS due to gain errors can severely impact the estimation of parameters, introducing bias. The sensitivity of derived parameters to gain errors clearly suggests that the gain error threshold should be much lower than 0.01%, ideally closer to 0.001%. If the gain error exceeds 0.001%, it is advisable to model them to prevent bias in the derived parameter values.

HERA: HERA, a crucial instrument for studying the Epoch of Reionization (EoR), has begun its observations and recently produced its first upper limit based on initial phase data [27]. To assess the impact of calibration errors on the observed power spectrum (PS) and the corresponding astrophysical parameters for HERA, we introduced various gain errors similar to those observed in SKA-Low. The residual power spectrum (PS) due to different gain errors is presented in the bottom left panels of Fig. 5, while the posterior distributions of model parameters derived from these PS measurements are shown in the bottom right panels of Fig. 5. Upon examining the residual PS spectrum, we found that when the gain error is 0.001%, the residual PS closely aligns with the true PS. But when the gain error increases to 0.01%, the residual PS overlaps with the true PS at lower k modes but diverges slightly at higher k modes.

The derived astrophysical parameters are consistent with the true PS for a gain error of 0.001%, but significant discrepancies emerge at a 0.01% gain error. This indicates that even minor deviations in the PS due to gain errors can considerably affect parameter estimation, leading to bias. Thus, it is essential for gain error thresholds to remain below 0.01%, ideally closer to 0.001%. If gain errors exceed 0.001%, they should be carefully modeled to avoid bias in the parameter values.

8.2.2 Position Error

To evaluate the impact of position errors in the global sky model, simulations were conducted using inaccurate sky models as described in [1]. Position errors were modeled with zero-mean Gaussian distributions and varying standard deviations (up to 0.048", 0.48", and 4.8") and applied to the right ascension (RA) of sources, resulting in a new catalog with positional

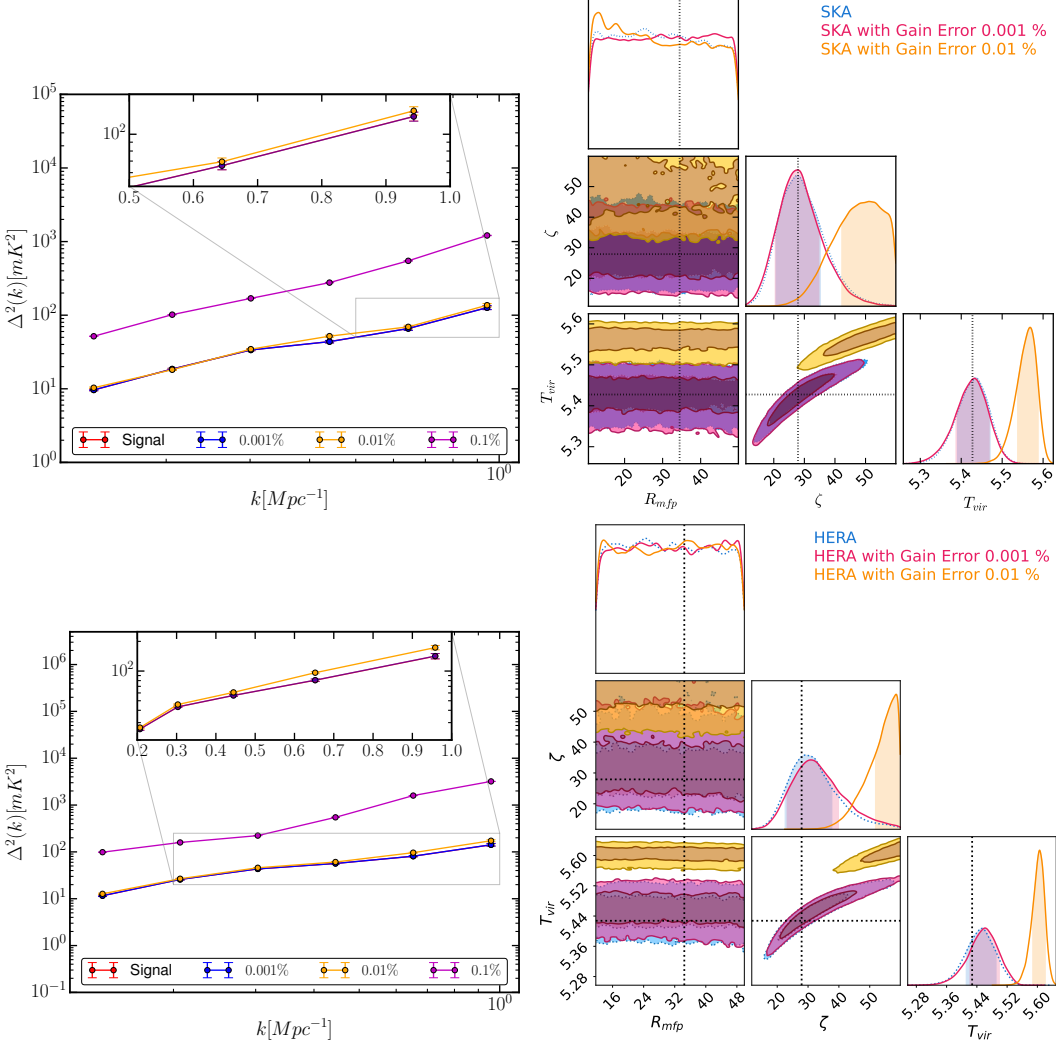


Figure 5. (Left) Residual power spectra for gain errors (0.001%, 0.01%, and 0.1%) compared to the signal power for different array layouts: SKA-Low (**top**) and HERA (**bottom**). Error bars represent 1σ uncertainties, including sample variance and thermal noise. **(Right)** Posterior distributions of model parameters from the power spectrum analysis (blue), with gain errors of 0.001% (magenta) and 0.01% (orange) for SKA-Low (**top**) and HERA (**bottom**). The shaded regions represent the 1σ and 2σ confidence intervals.

inaccuracies. Residuals were then obtained following equation 4 from [1], by subtracting the corrupted sky from the true sky, and these residuals were used to analyze the effects on the PS.

SKA Low: Similar to calibration errors, we evaluated the impact of position errors on the observed power spectrum (PS) and their effect on the inferred astrophysical parameters for SKA-Low. Different position errors, as described above, were introduced, and the resulting residual PS was compared with the true PS, as shown in the top-left panel of Fig. 6. The parameters obtained from the PS, which incorporates actual signals and position error residuals, are depicted in the top right panel of Fig. 6. Upon examining the plotted residual PS spectrum, we found that for a position error of $0.048''$, the residual PS overlaps with the

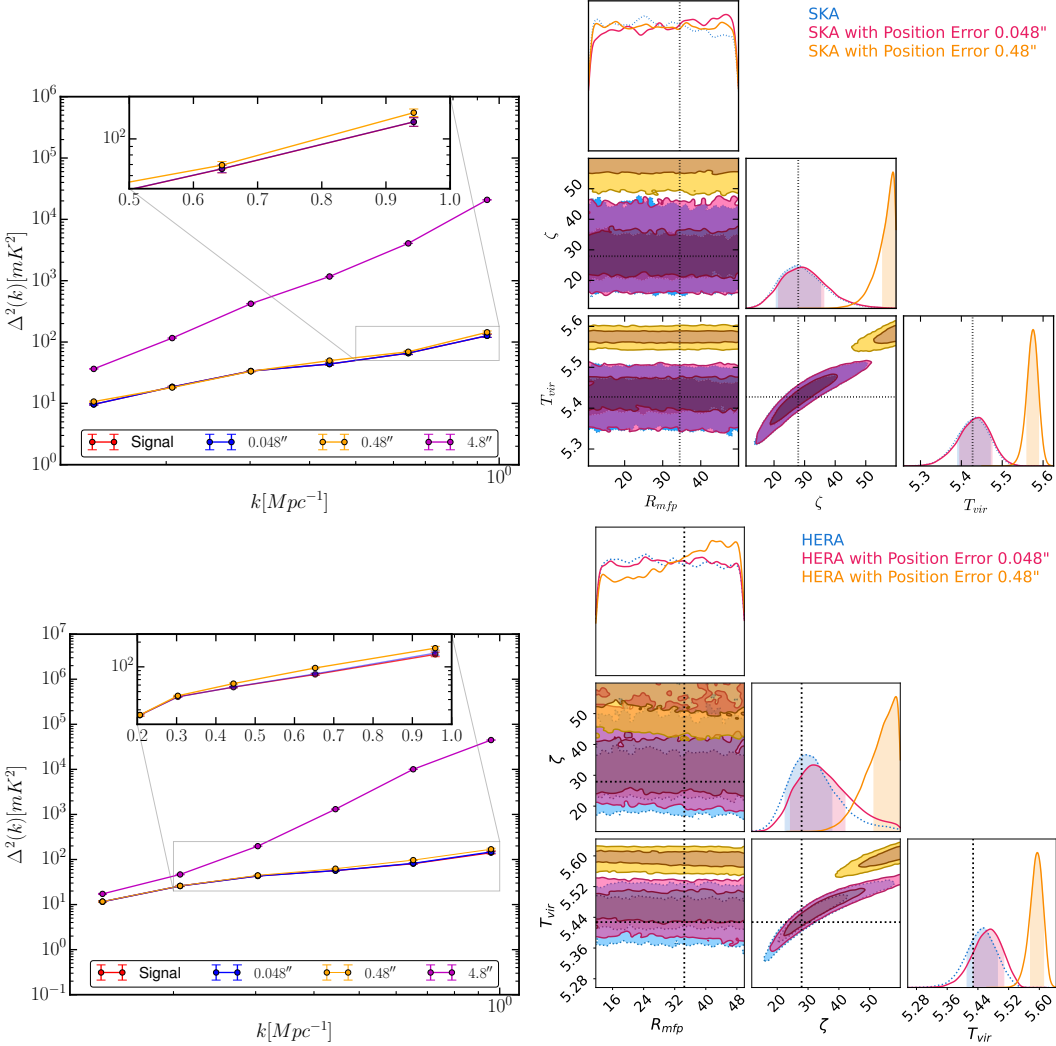


Figure 6. (Left) Residual power spectra for position errors (0.048", 0.48", and 4.8") for SKA-Low (top) and HERA (bottom). The error bars are 1σ uncertainties for the k -bins including sample variance and thermal noise. (Right) Posterior distributions of model parameters from residual power spectra for position errors of 0.048" (magenta) and 0.48" (orange), with SKA-Low, and HERA. The shaded regions represent the 1σ and 2σ confidence intervals.

true PS. At lower k modes, the residual PS with this position error overlaps well with the true PS, but at higher k modes, there is a minor deviation. This occurs because real-space scales are more affected by arcsecond-level errors at higher k values. However, since we used the entire k range to derive astrophysical parameters from the residual power spectrum, we observed that for a position error of 0.048", the derived parameters closely match those obtained from the true PS. Similarly, for a position error of 0.48", the derived parameters exhibit substantial deviations from the true values. This indicates that astrophysical parameters are highly sensitive to position errors, and even small deviations in the PS due to these errors can severely impact parameter estimation, introducing bias. The sensitivity of derived parameters to position errors, similar to gain errors, suggests that the acceptable position error threshold should be much lower than 0.48", ideally around 0.048". If the position error

exceeds $0.048''$, modeling the errors becomes crucial to prevent bias in the derived parameter values.

HERA : To assess the impact of position errors on the observed power spectrum (PS) and their influence on astrophysical parameters for HERA, we introduced various position errors similar to those in SKA-Low. The residual PS was visually compared with the actual PS, as shown in the bottom-left panel of Fig.6. The parameters obtained from the PS analysis, incorporating actual signal and PS for position error residuals, are depicted in the bottom-right panel of Fig.6. We observed that for position errors of $0.048''$, the residual PS overlaps with the true PS, with overlap at lower k modes and very minor deviations at higher k modes. However, for a position error of $0.48''$, the derived parameters significantly differed from the actual values, indicating high sensitivity to position errors. This suggests that the position error threshold should be much lower than $0.48''$, ideally closer to $0.048''$. If position errors exceed $0.048''$, they should be modeled to prevent bias in parameter estimation.

9 Summary and Discussion

This study presents the development of an ANN and Bayesian-based framework for inferring astrophysical parameters from observed HI power spectra (PS). We used the 21cm E2E pipeline to generate the mock observed power spectrum (PS) for different array configurations, including SKA Low core and HERA. However, generating a multitude of observable model signals across a multi-dimensional parameter space for Bayesian inference proved computationally difficult, especially with simulated observations. To address this, we adopted a formalism utilized by several groups, employing emulators for modelling the Epoch of Reionization (EoR) signal instead of actual simulations.

For constructing the training datasets of observed PS, EoR 21cm signals were generated using the semi-numerical simulation 21cmFAST, with key EoR parameters (R_{mfp} , T_{vir} , and ζ) described in section 2.1. These signals served as sky signals for mock observations using the 21cm E2E pipeline with various interferometric arrays like SKA Low and HERA, allowing us to construct sets of PS under different astrophysical conditions. These simulated observed PS were then used to train separate emulators for each interferometric array, facilitating Bayesian inference of the corresponding astrophysical parameters. A key advantage of these emulators, beyond conserving computational resources, is that our ANN-based models are trained directly on observed PS data while incorporating telescope effects. This allows for direct parameter inference without requiring separate corrections for telescope effects. In the first case of the study, we perform the inference using the developed ANN and Bayesian-based pipeline assuming perfect observing conditions where we assume the foreground had been perfectly removing only signal and telescope effect is there in the observed PS. We infer the astrophysical EoR parameters for the three sets for the signals constructed using the true astrophysical parameters, as listed in Tab.2. We have made the inference for the given different interferometers by considering the sample variance and the system noise at redshift $z = 9$ corresponding to 1000 hrs observation time for each given interferometric array individually, detail result listed in Tab.2. Additionally, we have inferred astrophysical parameters from theoretical power spectra (PS) and compared these findings with parameters inferred from observed PS. In all three cases, the inferred parameters T_{vir} and ζ closely matched the actual values, while the parameter R_{mfp} was often not well-constrained, indicating high degeneracy. In the second case of the study, we assumed that the foregrounds were not perfectly removed, leaving some residual foreground due to calibration or position errors. This study aimed to

determine the threshold level of calibration or position error for various interferometric arrays, such as SKA-Low and HERA. In a previous study by [1], 2D and 1D power spectra with gain and position errors were visually examined. They also calculated the root mean square (RMS) in the residual image across different percentage errors in calibration and position, comparing it with signal levels and thermal noise. They found the calibration error threshold to be 0.01 % and the position error threshold to be 0.48”.

In this study, we delve deeper and systematically analyze these effects by performing inference on the observed power spectra from different interferometers. This allows us to understand the impact of various calibration and position errors on astrophysical parameters. The key findings noted from this study:

- Our analysis showed that the calibration error threshold for SKA-Low is 0.001%. Exceeding this threshold results in significant deviations in the inferred astrophysical parameters from their actual values, severely affecting the astrophysical processes. Similarly, for HERA, the calibration error threshold is also 0.001%, and surpassing this threshold leads to notable discrepancies between the inferred and actual parameters.
- The position error threshold for SKA-Low and HERA is found to be $> 0.48''$, as displacements $\geq 0.48''$ cause significant deviations between the inferred astrophysical parameters and their actual values. This suggests that position errors can bias the inference of the astrophysical parameters.
- We also observed that, among all three parameters, ζ is the most sensitive to the power spectrum (PS). Even small variations in the PS, caused by calibration gain or position errors, have a significant impact on the ionization efficiency parameter, ζ .
- Among the two array layouts, we found that SKA Low exhibits slightly better tolerance than HERA for both calibration and position errors.

Thus, we conclude that for the existing interferometers, the calibration error should be nearly 0.001%, and the position error should be less than 0.48” to avoid biasing the inference. Beyond these thresholds, these errors start to affect the results. To reduce their impact, calibration must be performed with the same level of accuracy, or we need to develop modeling or mitigation techniques to eliminate the residual foregrounds arising from calibration or position errors, ensuring minimal influence on the inference. The simulations conducted in this study are based on several simplifying assumptions about foregrounds and instruments. The optimal tolerance for both calibration and position errors remains similar across both the scenarios. However, in the presence of calibration errors, SKA-Low’s power spectrum performance is slightly better than the HERA, with the inferred parameters more closely matching the actual values. This suggests the need for more detailed simulations, incorporating effects such as primary beam chromaticity, to better determine the optimal array configuration. Future studies will include these more complex simulations for a more comprehensive analysis.

A Robustness Evaluation of the Emulator-based MCMC Pipeline

Acknowledgments

AT would like to thank the Indian Institute of Technology Indore for providing funding for this study in the form of a Teaching Assistantship. SM and AD acknowledge financial

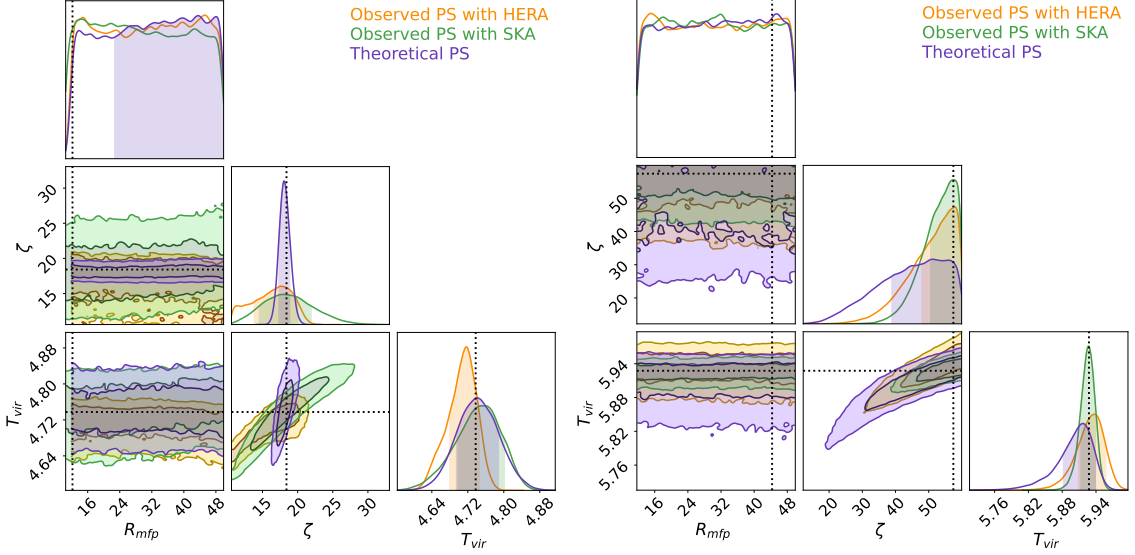


Figure 7. Depicts the posterior distribution of model parameters obtained through power spectrum analysis, comparing the theoretical power spectrum with the observed power spectrum using various interferometric arrays, including SKA-Low and HERA. The enclosed areas between the inner and outer contours signify the 1σ and 2σ confidence levels, respectively.

Set	Parameters & True value	Theoretical PS	Observed PS with SKA low	Observed PS with HERA
Set 1	R_{mfp} : 34.67	—	—	—
	ζ : 27.92	$27.5^{+3.7}_{-3.4}$	$27.76^{+7.5}_{-6.9}$	$29.1^{+8.6}_{-6.6}$
	T_{vir} : 5.428	$5.428^{+0.023}_{-0.032}$	$5.437^{+0.033}_{-0.046}$	$5.455^{+0.036}_{-0.043}$
Set 2	R_{mfp} : 12.2	50.0^{+0}_{-27}	—	—
	ζ : 18.42	$18.09^{+0.80}_{-0.75}$	$17.7^{+4.2}_{-3.2}$	$17.6^{+2.0}_{-2.7}$
	T_{vir} : 4.738	$4.734^{+0.046}_{-0.048}$	$4.761^{+0.041}_{-0.062}$	$4.721^{+0.029}_{-0.026}$
Set 3	R_{mfp} : 44.33	—	—	50.0^{+0}_{-26}
	ζ : 57.42	$50.8^{+9.0}_{-11.9}$	$59.8^{+0.0}_{-9.3}$	$59.40^{+0.41}_{-11.46}$
	T_{vir} : 5.928	$5.917^{+0.022}_{-0.035}$	$5.926^{+0.013}_{-0.013}$	$5.938^{+0.019}_{-0.030}$

Table 2. Inferred EoR model parameters (ζ , T_{vir} , and R_{mfp}) with 1σ uncertainties for different parameter sets. Theoretical power spectrum (PS) estimates are compared with observed PS constraints from SKA-Low and HERA.

support through the project titled “Observing the Cosmic Dawn in Multicolour using Next Generation Telescopes” funded by the Science and Engineering Research Board (SERB), Department of Science and Technology, Government of India through the Core Research Grant No. CRG/2021/004025. The authors acknowledge the use of facilities procured through the funding via the Department of Science and Technology, Government of India sponsored DST-FIST grant no. SR/FST/PSII/2021/162 (C) awarded to the DAASE, IIT Indore.

References

- [1] A. Mazumder, A. Datta, A. Chakraborty and S. Majumdar, *Observing the reionization: effect of calibration and position errors on realistic observation conditions*, *Monthly Notices of the Royal Astronomical Society* **515** (2022) 4020 [[2207.06169](https://arxiv.org/abs/2207.06169)].
- [2] G.B. Field, *Excitation of the hydrogen 21-cm line*, *Proceedings of the IRE* **46** (1958) 240.
- [3] G.B. Field, *The spin temperature of intergalactic neutral hydrogen.*, *The Astrophysical Journal* **129** (1959) 536.
- [4] G.B. Field, *The time relaxation of a resonance-line profile.*, *The Astrophysical Journal* **129** (1959) 551.
- [5] S.R. Furlanetto, S. Peng Oh and F.H. Briggs, *Cosmology at low frequencies: The 21cm transition and the high-redshift universe*, *Physics Reports* **433** (2006) 181.
- [6] M.F. Morales and J.S.B. Wyithe, *Reionization and cosmology with 21-cm fluctuations*, *Annual Review of Astronomy and Astrophysics* **48** (2010) 127 [<https://doi.org/10.1146/annurev-astro-081309-130936>].
- [7] J.R. Pritchard and A. Loeb, *21 cm cosmology in the 21st century*, *Reports on Progress in Physics* **75** (2012) 086901.
- [8] R. Barkana, *The rise of the first stars: Supersonic streaming, radiative feedback, and 21-cm cosmology*, *Physics Reports* **645** (2016) 1.
- [9] P. Dayal and A. Ferrara, *Early galaxy formation and its large-scale effects*, *Physics Reports* **780-782** (2018) 1.
- [10] X. Fan, C. Carilli and B. Keating, *Observational constraints on cosmic reionization*, *Annual Review of Astronomy and Astrophysics* **44** (2006) 415 [<https://doi.org/10.1146/annurev.astro.44.051905.092514>].
- [11] Planck Collaboration, Aghanim, N., Akrami, Y., Arroja, F., Ashdown, M., Aumont, J. et al., *Planck 2018 results. i. overview and the cosmological legacy of planck*, *A&A* (2019) .
- [12] S. Bharadwaj and S.K. Sethi, *HI Fluctuations at Large Redshifts: I–Visibility correlation*, *Journal of Astrophysics and Astronomy* **22** (2001) 293 [[astro-ph/0203269](https://arxiv.org/abs/astro-ph/0203269)].
- [13] S. Bharadwaj and S.S. Ali, *On using visibility correlations to probe the HI distribution from the dark ages to the present epoch - I. Formalism and the expected signal*, *Monthly Notices of the Royal Astronomical Society* **356** (2005) 1519 [[astro-ph/0406676](https://arxiv.org/abs/astro-ph/0406676)].
- [14] M.F. Morales, *Power Spectrum Sensitivity and the Design of Epoch of Reionization Observatories*, *The Astrophysical Journal* **619** (2005) 678 [[astro-ph/0406662](https://arxiv.org/abs/astro-ph/0406662)].
- [15] M. Zaldarriaga, S.R. Furlanetto and L. Hernquist, *21 Centimeter Fluctuations from Cosmic Gas at High Redshifts*, *The Astrophysical Journal* **608** (2004) 622 [[astro-ph/0311514](https://arxiv.org/abs/astro-ph/0311514)].
- [16] J.D. Bowman, A.E.E. Rogers, R.A. Monsalve, T.J. Mozdzen and N. Mahesh, *An absorption profile centred at 78 megahertz in the sky-averaged spectrum*, *Nature* **555** (2018) 67.
- [17] S. Singh and R. Subrahmanyan, *The redshifted 21 cm signal in the EDGES low-band spectrum*, *The Astrophysical Journal* **880** (2019) 26.

- [18] S. Singh, N.T. Jishnu, R. Subrahmanyam, N. Udaya Shankar, B.S. Girish, A. Raghunathan et al., *On the detection of a cosmic dawn signal in the radio background*, *Nature Astronomy* **6** (2022) 607 [[2112.06778](https://arxiv.org/abs/2112.06778)].
- [19] M. Sokolowski, S.E. Tremblay, R.B. Wayth, S.J. Tingay, N. Clarke, P. Roberts et al., *Bighorns - broadband instrument for global hydrogen reionisation signal*, *Publications of the Astronomical Society of Australia* **32** (2015) e004.
- [20] T.C. Voytek, A. Natarajan, J.M.J. García, J.B. Peterson and O. López-Cruz, *PROBING THE DARK AGES AT $z \sim 20$: THE SCI-HI 21 cm ALL-SKY SPECTRUM EXPERIMENT*, *The Astrophysical Journal* **782** (2014) L9.
- [21] D.C. Price, L.J. Greenhill, A. Fialkov, G. Bernardi, H. Garsden, B.R. Barsdell et al., *Design and characterization of the Large-aperture Experiment to Detect the Dark Age (LEDA) radiometer systems*, *Monthly Notices of the Royal Astronomical Society* **478** (2018) 4193 [<https://academic.oup.com/mnras/article-pdf/478/3/4193/25097057/sty1244.pdf>].
- [22] G. Paciga, T.-C. Chang, Y. Gupta, R. Nityanada, J. Odegova, U.-L. Pen et al., *The GMRT Epoch of Reionization experiment: a new upper limit on the neutral hydrogen power spectrum at $z \approx 8.6$* , *Monthly Notices of the Royal Astronomical Society* **413** (2011) 1174.
- [23] A.P. Beardsley, B.J. Hazelton, I.S. Sullivan, P. Carroll, N. Barry, M. Rahimi et al., *FIRST SEASON MWA EOR POWER SPECTRUM RESULTS AT REDSHIFT 7*, *The Astrophysical Journal* **833** (2016) 102.
- [24] B.K. Gehlot, F.G. Mertens, L.V.E. Koopmans, M.A. Brentjens, S. Zaroubi, B. Ciardi et al., *The first power spectrum limit on the 21-cm signal of neutral hydrogen during the Cosmic Dawn at $z = 20-25$ from LOFAR*, *Monthly Notices of the Royal Astronomical Society* **488** (2019) 4271 [<http://oup.prod.sis.lan/mnras/article-pdf/488/3/4271/29110599/stz1937.pdf>].
- [25] C.M. Trott, C.H. Jordan, S. Midgley, N. Barry, B. Greig, B. Pindor et al., *Deep multiredshift limits on Epoch of Reionization 21 cm power spectra from four seasons of Murchison Widefield Array observations*, *Monthly Notices of the Royal Astronomical Society* **493** (2020) 4711 [<https://academic.oup.com/mnras/article-pdf/493/4/4711/32927265/staa414.pdf>].
- [26] F.G. Mertens, M. Mevius, L.V.E. Koopmans, A.R. Offringa, G. Mellema, S. Zaroubi et al., *Improved upper limits on the 21cm signal power spectrum of neutral hydrogen at $z \approx 9.1$ from LOFAR*, *Monthly Notices of the Royal Astronomical Society* **493** (2020) 1662 [<https://academic.oup.com/mnras/article-pdf/493/2/1662/32666766/staa327.pdf>].
- [27] The HERA Collaboration, Z. Abdurashidova, J.E. Aguirre, P. Alexander, Z.S. Ali, Y. Balfour et al., *First Results from HERA Phase I: Upper Limits on the Epoch of Reionization 21 cm Power Spectrum*, *arXiv e-prints* (2021) arXiv:2108.02263 [[2108.02263](https://arxiv.org/abs/2108.02263)].
- [28] V. Jelić, S. Zaroubi, P. Labropoulos, R.M. Thomas, G. Bernardi, M.A. Brentjens et al., *Foreground simulations for the LOFAR-epoch of reionization experiment*, *MNRAS* **389** (2008) 1319 [<http://oup.prod.sis.lan/mnras/article-pdf/389/3/1319/3338764/mnras0389-1319.pdf>].
- [29] V. Jelić, S. Zaroubi, P. Labropoulos, G. Bernardi, A.G. de Bruyn and L.V.E. Koopmans, *Realistic simulations of the Galactic polarized foreground: consequences for 21-cm reionization detection experiments*, *MNRAS* **409** (2010) 1647 [<http://oup.prod.sis.lan/mnras/article-pdf/409/4/1647/3087131/mnras0409-1647.pdf>].
- [30] O. Zahn, A. Mesinger, M. McQuinn, H. Trac, R. Cen and L.E. Hernquist, *Comparison of reionization models: radiative transfer simulations and approximate, seminumeric models*, *Monthly Notices of the Royal Astronomical Society* **414** (2011) 727 [<https://academic.oup.com/mnras/article-pdf/414/1/727/3838580/mnras0414-0727.pdf>].
- [31] E. Chapman, A. Bonaldi, G. Harker, V. Jelic, F.B. Abdalla, G. Bernardi et al., *Cosmic dawn and epoch of reionization foreground removal with the ska*, in *Advancing Astrophysics with the*

- Square Kilometre Array (AASKA14)*, p. 5, Apr, 2015,
<https://ui.adsabs.harvard.edu/abs/2015aska.confE...5C>.
- [32] S. Choudhuri, S. Bharadwaj, S.S. Ali, N. Roy, H.T. Intema and A. Ghosh, *The angular power spectrum measurement of the Galactic synchrotron emission in two fields of the TGSS survey*, *Monthly Notices of the Royal Astronomical Society: Letters* **470** (2017) L11
[\[https://academic.oup.com/mnrasl/article-pdf/470/1/L11/17657316/slx066.pdf\]](https://academic.oup.com/mnrasl/article-pdf/470/1/L11/17657316/slx066.pdf).
- [33] A. Chakraborty, N. Roy, A. Datta, S. Choudhuri, K.K. Datta, P. Dutta et al., *Detailed study of ELAIS N1 field with the uGMRT – II. Source properties and spectral variation of foreground power spectrum from 300–500 MHz observations*, *Monthly Notices of the Royal Astronomical Society* **490** (2019) 243
[\[http://oup.prod.sis.lan/mnras/article-pdf/490/1/243/30100389/stz2533.pdf\]](http://oup.prod.sis.lan/mnras/article-pdf/490/1/243/30100389/stz2533.pdf).
- [34] A. Mazumder, A. Chakraborty, A. Datta, S. Choudhuri, N. Roy, Y. Wadadekar et al., *Characterizing EoR foregrounds: a study of the Lockman Hole region at 325 MHz*, *Monthly Notices of the Royal Astronomical Society* **495** (2020) 4071
[\[https://academic.oup.com/mnras/article-pdf/495/4/4071/33371252/staa1317.pdf\]](https://academic.oup.com/mnras/article-pdf/495/4/4071/33371252/staa1317.pdf).
- [35] A. Datta, J.D. Bowman and C.L. Carilli, *BRIGHT SOURCE SUBTRACTION REQUIREMENTS FOR REDSHIFTED 21 cm MEASUREMENTS*, *The Astrophysical Journal* **724** (2010) 526.
- [36] C.M. Trott, R.B. Wayth and S.J. Tingay, *THE IMPACT OF POINT-SOURCE SUBTRACTION RESIDUALS ON 21 cm EPOCH OF REIONIZATION ESTIMATION*, *The Astrophysical Journal* **757** (2012) 101.
- [37] E. Chapman, S. Zaroubi, F.B. Abdalla, F. Dulwich, V. Jelić and B. Mort, *The effect of foreground mitigation strategy on EoR window recovery*, *Monthly Notices of the Royal Astronomical Society* **458** (2016) 2928
[\[https://academic.oup.com/mnras/article-pdf/458/3/2928/8004887/stw161.pdf\]](https://academic.oup.com/mnras/article-pdf/458/3/2928/8004887/stw161.pdf).
- [38] H. Vedantham, N.U. Shankar and R. Subrahmanyan, *IMAGING THE EPOCH OF REIONIZATION: LIMITATIONS FROM FOREGROUND CONFUSION AND IMAGING ALGORITHMS*, *The Astrophysical Journal* **745** (2012) 176.
- [39] N. Thyagarajan, D.C. Jacobs, J.D. Bowman, N. Barry, A.P. Beardsley, G. Bernardi et al., *FOREGROUNDS IN WIDE-FIELD REDSHIFTED 21 cm POWER SPECTRA*, *The Astrophysical Journal* **804** (2015) 14.
- [40] N. Thyagarajan, D.C. Jacobs, J.D. Bowman, N. Barry, A.P. Beardsley, G. Bernardi et al., *CONFIRMATION OF WIDE-FIELD SIGNATURES IN REDSHIFTED 21 cm POWER SPECTRA*, *The Astrophysical Journal* **807** (2015) L28.
- [41] F.G. Mertens, A. Ghosh and L.V.E. Koopmans, *Statistical 21-cm signal separation via Gaussian Process Regression analysis*, *Monthly Notices of the Royal Astronomical Society* **478** (2018) 3640
[\[https://academic.oup.com/mnras/article-pdf/478/3/3640/25072259/sty1207.pdf\]](https://academic.oup.com/mnras/article-pdf/478/3/3640/25072259/sty1207.pdf).
- [42] I. Hothi, E. Chapman, J.R. Pritchard, F.G. Mertens, L.V.E. Koopmans, B. Ciardi et al., *Comparing foreground removal techniques for recovery of the LOFAR-EoR 21cm power spectrum*, *Monthly Notices of the Royal Astronomical Society* **500** (2020) 2264
[\[https://academic.oup.com/mnras/article-pdf/500/2/2264/34497733/staa3446.pdf\]](https://academic.oup.com/mnras/article-pdf/500/2/2264/34497733/staa3446.pdf).
- [43] E. de Lera Acedo, C.M. Trott, R.B. Wayth, N. Fagnoni, G. Bernardi, B. Wakley et al., *Spectral performance of SKA Log-periodic Antennas I: mitigating spectral artefacts in SKA1-LOW 21 cm cosmology experiments*, *Monthly Notices of the Royal Astronomical Society* **469** (2017) 2662
[\[https://academic.oup.com/mnras/article-pdf/469/3/2662/17628405/stx904.pdf\]](https://academic.oup.com/mnras/article-pdf/469/3/2662/17628405/stx904.pdf).

- [44] C.M. Trott, E. de Lera Acedo, R.B. Wayth, N. Fagnoni, A.T. Sutinjo, B. Wakley et al., *Spectral performance of Square Kilometre Array Antennas – II. Calibration performance*, *Monthly Notices of the Royal Astronomical Society* **470** (2017) 455
[\[https://academic.oup.com/mnras/article-pdf/470/1/455/17827642/stx1224.pdf\]](https://academic.oup.com/mnras/article-pdf/470/1/455/17827642/stx1224.pdf).
- [45] R.C. Joseph, C.M. Trott and R.B. Wayth, *The bias and uncertainty of redundant and sky-based calibration under realistic sky and telescope conditions*, *The Astronomical Journal* **156** (2018) 285.
- [46] W. Li, J.C. Pober, B.J. Hazelton, N. Barry, M.F. Morales, I. Sullivan et al., *Comparing redundant and sky-model-based interferometric calibration: A first look with phase II of the MWA*, *The Astrophysical Journal* **863** (2018) 170.
- [47] A.R. Offringa, R.B. Wayth, N. Hurley-Walker, D.L. Kaplan, N. Barry, A.P. Beardsley et al., *The low-frequency environment of the murchison widefield array: Radio-frequency interference analysis and mitigation*, *Publications of the Astronomical Society of Australia* **32** (2015) e008.
- [48] N. Barry, B. Hazelton, I. Sullivan, M.F. Morales and J.C. Pober, *Calibration requirements for detecting the 21 cm epoch of reionization power spectrum and implications for the SKA*, *Monthly Notices of the Royal Astronomical Society* **461** (2016) 3135
[\[https://academic.oup.com/mnras/article-pdf/461/3/3135/8106921/stw1380.pdf\]](https://academic.oup.com/mnras/article-pdf/461/3/3135/8106921/stw1380.pdf).
- [49] C.M. Trott and R.B. Wayth, *Spectral calibration requirements of radio interferometers for epoch of reionisation science with the ska*, *Publications of the Astronomical Society of Australia* **33** (2016) e019.
- [50] A. Ewall-Wice, J.S. Dillon, A. Liu and J. Hewitt, *The impact of modelling errors on interferometer calibration for 21 cm power spectra*, *Monthly Notices of the Royal Astronomical Society* **470** (2017) 1849
[\[https://academic.oup.com/mnras/article-pdf/470/2/1849/18139300/stx1221.pdf\]](https://academic.oup.com/mnras/article-pdf/470/2/1849/18139300/stx1221.pdf).
- [51] A.H. Patil, S. Yatawatta, L.V.E. Koopmans, A.G. de Bruyn, M.A. Brentjens, S. Zaroubi et al., *Upper limits on the 21 cm epoch of reionization power spectrum from one night with LOFAR*, *The Astrophysical Journal* **838** (2017) 65.
- [52] J.S. Dillon, S.A. Kohn, A.R. Parsons, J.E. Aguirre, Z.S. Ali, G. Bernardi et al., *Polarized redundant-baseline calibration for 21cm cosmology without adding spectral structure*, *Monthly Notices of the Royal Astronomical Society* **477** (2018) 5670
[\[https://academic.oup.com/mnras/article-pdf/477/4/5670/24955748/sty1060.pdf\]](https://academic.oup.com/mnras/article-pdf/477/4/5670/24955748/sty1060.pdf).
- [53] N.S. Kern, A.R. Parsons, J.S. Dillon, A.E. Lanman, N. Fagnoni and E. de Lera Acedo, *Mitigating internal instrument coupling for 21 cm cosmology. i. temporal and spectral modeling in simulations*, *The Astrophysical Journal* **884** (2019) 105.
- [54] J. Kumar, P. Dutta and N. Roy, *Calibration requirements for epoch of reionization 21-cm signal observations – I. Effect of time-correlated gains*, *Monthly Notices of the Royal Astronomical Society* **495** (2020) 3683
[\[https://academic.oup.com/mnras/article-pdf/495/4/3683/33347813/staa1371.pdf\]](https://academic.oup.com/mnras/article-pdf/495/4/3683/33347813/staa1371.pdf).
- [55] C.H. Jordan, S. Murray, C.M. Trott, R.B. Wayth, D.A. Mitchell, M. Rahimi et al., *Characterization of the ionosphere above the Murchison Radio Observatory using the Murchison Widefield Array*, *Monthly Notices of the Royal Astronomical Society* **471** (2017) 3974
[\[https://academic.oup.com/mnras/article-pdf/471/4/3974/19558756/stx1797.pdf\]](https://academic.oup.com/mnras/article-pdf/471/4/3974/19558756/stx1797.pdf).
- [56] C.M. Trott, C.H. Jordan, S.G. Murray, B. Pindor, D.A. Mitchell, R.B. Wayth et al., *Assessment of ionospheric activity tolerances for epoch of reionization science with the murchison widefield array*, *The Astrophysical Journal* **867** (2018) 15.
- [57] S.K. Pal, A. Datta and A. Mazumder, *Ionospheric effect on the synthetic Epoch of*

- Reionization observations with the SKA1-Low*, *arXiv e-prints* (2024) arXiv:2407.17573 [2407.17573].
- [58] D.R. DeBoer, A.R. Parsons, J.E. Aguirre, P. Alexander, Z.S. Ali, A.P. Beardsley et al., *Hydrogen epoch of reionization array (HERA)*, *Publications of the Astronomical Society of the Pacific* **129** (2017) 045001.
- [59] L. Koopmans, J. Pritchard, G. Mellema, J. Aguirre, K. Ahn, R. Barkana et al., *The Cosmic Dawn and Epoch of Reionisation with SKA*, in *Advancing Astrophysics with the Square Kilometre Array (AASKA14)*, p. 1, Apr., 2015, DOI [1505.07568].
- [60] G. Mellema, L. Koopmans, H. Shukla, K.K. Datta, A. Mesinger and S. Majumdar, *HI tomographic imaging of the Cosmic Dawn and Epoch of Reionization with SKA*, in *Advancing Astrophysics with the Square Kilometre Array (AASKA14)*, PoS, 2014, DOI.
- [61] M.F. Morales and J. Hewitt, *Toward epoch of reionization measurements with wide-field radio observations*, *The Astrophysical Journal* **615** (2004) 7.
- [62] M.F. Morales, J.D. Bowman and J.N. Hewitt, *Improving foreground subtraction in statistical observations of 21 cm emission from the epoch of reionization*, *The Astrophysical Journal* **648** (2006) 767.
- [63] J.D. Bowman, M.F. Morales and J.N. Hewitt, *FOREGROUND CONTAMINATION IN INTERFEROMETRIC MEASUREMENTS OF THE REDSHIFTED 21 cm POWER SPECTRUM*, *The Astrophysical Journal* **695** (2009) 183.
- [64] A. Liu and M. Tegmark, *A method for 21 cm power spectrum estimation in the presence of foregrounds*, *Phys. Rev. D* **83** (2011) 103006.
- [65] A. Parsons, J. Pober, M. McQuinn, D. Jacobs and J. Aguirre, *A SENSITIVITY AND ARRAY-CONFIGURATION STUDY FOR MEASURING THE POWER SPECTRUM OF 21 cm EMISSION FROM REIONIZATION*, *The Astrophysical Journal* **753** (2012) 81.
- [66] J.C. Pober, A.R. Parsons, D.R. DeBoer, P. McDonald, M. McQuinn, J.E. Aguirre et al., *The baryon acoustic oscillation broadband and broad-beam array: Design overview and sensitivity forecasts*, *The Astronomical Journal* **145** (2013) 65.
- [67] J.S. Dillon, A. Liu and M. Tegmark, *A fast method for power spectrum and foreground analysis for 21 cm cosmology*, *Phys. Rev. D* **87** (2013) 043005.
- [68] M.F. Morales, B. Hazelton, I. Sullivan and A. Beardsley, *FOUR FUNDAMENTAL FOREGROUND POWER SPECTRUM SHAPES FOR 21 cm COSMOLOGY OBSERVATIONS*, *The Astrophysical Journal* **752** (2012) 137.
- [69] A. Datta, S. Bhatnagar and C.L. Carilli, *DETECTION OF SIGNALS FROM COSMIC REIONIZATION USING RADIO INTERFEROMETRIC SIGNAL PROCESSING*, *The Astrophysical Journal* **703** (2009) 1851.
- [70] R. Byrne, M.F. Morales, B. Hazelton, W. Li, N. Barry, A.P. Beardsley et al., *Fundamental limitations on the calibration of redundant 21 cm cosmology instruments and implications for HERA and the SKA*, *The Astrophysical Journal* **875** (2019) 70.
- [71] R. Byrne, M.F. Morales, B. Hazelton and M. Wilensky, *A unified calibration framework for 21 cm cosmology*, Apr, 2020.
- [72] A. Cohen, A. Fialkov, R. Barkana and R.A. Monsalve, *Emulating the global 21-cm signal from Cosmic Dawn and Reionization*, *Monthly Notices of the Royal Astronomical Society* **495** (2020) 4845 [1910.06274].
- [73] H.T.J. Bevins, W.J. Handley, A. Fialkov, E. de Lera Acedo and K. Javid, *globalemu: a novel and robust approach for emulating the sky-averaged 21-cm signal from the cosmic dawn and epoch of reionization*, *Monthly Notices of the Royal Astronomical Society* **508** (2021) 2923 [https://academic.oup.com/mnras/article-pdf/508/2/2923/40634384/stab2737.pdf].

- [74] C.H. Bye, S.K.N. Portillo and A. Fialkov, *21cmVAE: A Very Accurate Emulator of the 21 cm Global Signal*, *The Astrophysical Journal* **930** (2022) 79 [[2107.05581](#)].
- [75] C.J. Schmit and J.R. Pritchard, *Emulation of reionization simulations for Bayesian inference of astrophysics parameters using neural networks*, *Monthly Notices of the Royal Astronomical Society* **475** (2018) 1213 [[1708.00011](#)].
- [76] H. Tiwari, A.K. Shaw, S. Majumdar, M. Kamran and M. Choudhury, *Improving constraints on the reionization parameters using 21-cm bispectrum*, *Journal of Cosmology and Astroparticle Physics* **2022** (2022) 045 [[2108.07279](#)].
- [77] M. Choudhury, A. Datta and A. Chakraborty, *Extracting the 21 cm Global signal using artificial neural networks*, *Monthly Notices of the Royal Astronomical Society* **491** (2020) 4031 [[1911.02580](#)].
- [78] M. Choudhury, A. Chatterjee, A. Datta and T.R. Choudhury, *Using artificial neural networks to extract the 21-cm global signal from the EDGES data*, *Monthly Notices of the Royal Astronomical Society* **502** (2021) 2815 [[2012.00028](#)].
- [79] A. Tripathi, A. Datta, M. Choudhury and S. Majumdar, *Extracting the Global 21-cm signal from Cosmic Dawn and Epoch of Reionization in the presence of Foreground and Ionosphere*, *Monthly Notices of the Royal Astronomical Society* **528** (2024) 1945 [<https://academic.oup.com/mnras/article-pdf/528/2/1945/56437820/stae078.pdf>].
- [80] A. Tripathi, G. Kaur, A. Datta and S. Majumdar, *Comparing sampling techniques to chart parameter space of 21 cm global signal with Artificial Neural Networks*, *Journal of Cosmology and Astroparticle Physics* **2024** (2024) 041 [[2406.15832](#)].
- [81] H. Shimabukuro and B. Semelin, *Analysing the 21 cm signal from the epoch of reionization with artificial neural networks*, *Monthly Notices of the Royal Astronomical Society* **468** (2017) 3869 [[1701.07026](#)].
- [82] M. Choudhury, A. Datta and S. Majumdar, *Extracting the 21-cm power spectrum and the reionization parameters from mock data sets using artificial neural networks*, *Monthly Notices of the Royal Astronomical Society* **512** (2022) 5010 [[2112.13866](#)].
- [83] S. Hassan, A. Liu, S. Kohn and P. La Plante, *Identifying reionization sources from 21 cm maps using Convolutional Neural Networks*, *Monthly Notices of the Royal Astronomical Society* **483** (2019) 2524 [[1807.03317](#)].
- [84] J. Chardin, G. Uhrlrich, D. Aubert, N. Deparis, N. Gillet, P. Ocvirk et al., *A deep learning model to emulate simulations of cosmic reionization*, *Monthly Notices of the Royal Astronomical Society* **490** (2019) 1055 [[1905.06958](#)].
- [85] N. Gillet, A. Mesinger, B. Greig, A. Liu and G. Ucci, *Deep learning from 21-cm tomography of the cosmic dawn and reionization*, *Monthly Notices of the Royal Astronomical Society* **484** (2019) 282 [[1805.02699](#)].
- [86] W.D. Jennings, C.A. Watkinson, F.B. Abdalla and J.D. McEwen, *Evaluating machine learning techniques for predicting power spectra from reionization simulations*, *Monthly Notices of the Royal Astronomical Society* **483** (2019) 2907 [[1811.09141](#)].
- [87] W. Li, H. Xu, Z. Ma, R. Zhu, D. Hu, Z. Zhu et al., *Separating the EoR signal with a convolutional denoising autoencoder: a deep-learning-based method*, *Monthly Notices of the Royal Astronomical Society* **485** (2019) 2628 [[1902.09278](#)].
- [88] A. Mesinger, S. Furlanetto and R. Cen, *21CMFAST: a fast, seminumerical simulation of the high-redshift 21-cm signal*, *Monthly Notices of the Royal Astronomical Society* **411** (2011) 955 [[1003.3878](#)].
- [89] S. Murray, B. Greig, A. Mesinger, J. Muñoz, Y. Qin, J. Park et al., *21cmFAST v3: A*

- Python-integrated C code for generating 3D realizations of the cosmic 21cm signal., *The Journal of Open Source Software* **5** (2020) 2582 [2010.15121].*
- [90] M. McQuinn, S.P. Oh and C.-A. Faucher-Giguère, *On Lyman-limit Systems and the Evolution of the Intergalactic Ionizing Background*, *The Astrophysical Journal* **743** (2011) 82 [1101.1964].
- [91] E. Sobacchi and A. Mesinger, *Inhomogeneous recombinations during cosmic reionization*, *Monthly Notices of the Royal Astronomical Society* **440** (2014) 1662 [1402.2298].
- [92] E. Sobacchi and A. Mesinger, *How does radiative feedback from an ultraviolet background impact reionization?*, *Monthly Notices of the Royal Astronomical Society* **432** (2013) 3340 [1301.6781].
- [93] A. Fialkov, R. Barkana, E. Visbal, D. Tseliakhovich and C.M. Hirata, *The 21-cm signature of the first stars during the Lyman-Werner feedback era*, *Monthly Notices of the Royal Astronomical Society* **432** (2013) 2909 [1212.0513].
- [94] S.R. Furlanetto, M. Zaldarriaga and L. Hernquist, *The Growth of H II Regions During Reionization*, *The Astrophysical Journal* **613** (2004) 1 [astro-ph/0403697].
- [95] S.R. Furlanetto, S.P. Oh and F.H. Briggs, *Cosmology at low frequencies: The 21 cm transition and the high-redshift Universe*, *Physics Reports* **433** (2006) 181 [astro-ph/0608032].
- [96] A. Bonaldi, M. Bonato, V. Galluzzi, I. Harrison, M. Massardi, S. Kay et al., *The Tiered Radio Extragalactic Continuum Simulation (T-RECS)*, *Monthly Notices of the Royal Astronomical Society* **482** (2018) 2 [http://oup.prod.sis.lan/mnras/article-pdf/482/1/2/26081904/sty2603.pdf].
- [97] *Wide Field Astronomy & Technology for the Square Kilometre Array*, Jan., 2009.
- [98] *Wide Field Astronomy & Technology for the Square Kilometre Array*, Jan., 2009.
- [99] G. Mellema, L.V.E. Koopmans, F.A. Abdalla, G. Bernardi, B. Ciardi, S. Daiboo et al., *Reionization and the Cosmic Dawn with the Square Kilometre Array*, *Experimental Astronomy* **36** (2013) 235 [1210.0197].
- [100] G.B. Taylor, C.L. Carilli and R.A. Perley, *Synthesis imaging in radio astronomy ii, Synthesis Imaging in Radio Astronomy II* **180** (1999) .
- [101] F. Pedregosa, G. Varoquaux, A. Gramfort, V. Michel, B. Thirion, O. Grisel et al., *Scikit-learn: Machine Learning in Python*, *Journal of Machine Learning Research* **12** (2011) 2825 [1201.0490].
- [102] J. Akeret, S. Seehars, A. Amara, A. Refregier and A. Csillaghy, *CosmoHammer: Cosmological parameter estimation with the MCMC Hammer*, *arXiv e-prints* (2012) arXiv:1212.1721 [1212.1721].
- [103] J. Goodman and J. Weare, *Ensemble samplers with affine invariance*, *Communications in Applied Mathematics and Computational Science* **5** (2010) 65.
- [104] M. McQuinn, O. Zahn, M. Zaldarriaga, L. Hernquist and S.R. Furlanetto, *Cosmological Parameter Estimation Using 21 cm Radiation from the Epoch of Reionization*, *The Astrophysical Journal* **653** (2006) 815 [astro-ph/0512263].
- [105] G. Mellema, L.V.E. Koopmans, F.A. Abdalla, G. Bernardi, B. Ciardi, S. Daiboo et al., *Reionization and the Cosmic Dawn with the Square Kilometre Array*, *Experimental Astronomy* **36** (2013) 235 [1210.0197].